

Spatial gradient and quantitative attribution of karst soil erosion in Southwest China

Jiangbo Gao  · Huan Wang · Liyuan Zuo

Received: 2 July 2018 / Accepted: 12 November 2018
© Springer Nature Switzerland AG 2018

Abstract Soil erosion estimation has attracted considerable attention from the scientific community and governments because of its importance to sustainable regional development. In karst areas, the heterogeneous environment and rocky desertification create difficulties in determining the influencing factors and spatial patterns of soil erosion. A quantitative analysis of karst soil erosion distribution was conducted by applying the revised soil loss equation model and the geographical detector method of attribution identification, which was based on spatial variance analysis. The results show that soil erosion was most severe in areas with an elevation of 1200–1800 m and intense anthropogenic activity. When the vegetation coverage was below 0.5–0.6, soil erosion showed characteristics of a source-limited regime and increased with the increasing vegetation coverage. When the vegetation coverage was higher than 0.5–0.6, soil erosion followed a transport-limited regime

and decreased with the increasing vegetation coverage. The factor detector showed land use to be the dominant factor, explaining 51% of soil erosion distribution. Among various land use types, dry land had the greatest vulnerability to soil erosion. Slope served as a controlling factor at large scales, especially when combined with annual precipitation exceeding 1500 mm, and in dry and grassland areas. From the attribution analysis of multiple factors, the combination of land use and slope was the controlling interaction factor explaining 68% of soil erosion distribution. The methods and results of this research could serve as scientific references for decision makers and researchers exploring the characteristics of soil erosion to develop effective measures for its control.

Keywords Geographical detectors · RUSLE model · Soil erosion determinants · Spatial consistence · Spatial distribution

Huan Wang is the first co-author who contributed equally to this work

Electronic supplementary material The online version of this article (<https://doi.org/10.1007/s10661-018-7116-2>) contains supplementary material, which is available to authorized users.

J. Gao (✉) · H. Wang · L. Zuo
Key Laboratory of Land Surface Pattern and Simulation, Institute of Geographic Sciences and Natural Resources Research, Chinese Academy of Sciences, Beijing, China
e-mail: gaojiangbo@igsnrr.ac.cn

H. Wang · L. Zuo
College of Resources and Environment, University of Chinese Academy of Sciences, Beijing, China

Introduction

Soil erosion in terrestrial ecosystems is one of the most intractable problems facing the global community (Fu et al. 2011) threatening natural resources, environmental quality, and food security, and ultimately impeding sustainable regional development (Hu et al. 2015). Nevertheless, it is difficult to control the speed of soil loss due to the complex interplay of natural and anthropogenic factors, including soil properties, topography, climate change, and land use (Peng and Wang 2012; Wang et al. 2016). Assessing soil erosion and identifying its

influencing factors are major challenges that have become important topics in the fields of soil science, ecology, and geology (Fu et al. 2012, 2011; Markose and Jayappa 2016). In recent years, soil erosion assessment has been conducted in various regions, including ecologically fragile areas, such as Tibetan Plateau (Fang et al. 2015), karst areas (Dai et al. 2017b), and the Loess Plateau (Fu et al. 2010). It has also been carried out in areas of natural resource protection, including those with a high incidence of wild fire (Miller et al. 2003); in the agriculture production areas, such as the Northeast (Wang et al. 2014) and North China Plains (Yu et al. 2016); and in the key economic zones of the Yangtze (Long et al. 2016) and Pearl River Deltas (Xu et al. 2011).

Karst mountains are an important landscape globally and occupy 12% of continental terrain (Febles-Gonzalez et al. 2012). In the karst region of Southwest China, the topography changes over short distances, the ecosystem is very fragile, and the anthropogenic impact on the environment is significant because of the shallow soils and risk of rocky desertification (Feng et al. 2016). Rocky desertification is the main environmental and resource problem impeding social development, and results from uninhibited human activity and the lack of effective management (Parise et al. 2008). Soil erosion is the most important contributing factor to the karst region's rocky desertification. For this reason, extensive research on soil erosion monitoring, simulation, and prediction has been conducted in the karst regions of China (Dai et al. 2017a; Zeng et al. 2017).

To date, the focus has been on the spatial patterns of soil erosion and their correlation with land use and slope gradient (Chen et al. 2012; Wang et al. 2013; Xu et al. 2008). Several studies showed that soil erosion increased with slope and slope length, and that erosion could be reduced by using cross-slope cultivation rather than downslope tillage (Li et al. 2014; Xu et al. 2010). Therefore, quantitatively investigating the multifactorial influence of parameters such as slope and land use type is both meaningful and necessary. However, most studies have focused on single factors and have ignored multifactorial interactions, as well as integrated and quantitative attribution analysis. Here, we have applied the geographical detector method based on spatial variance analysis to investigate the quantitative attribution of factors influencing soil erosion, including both single factors and multifactorial interactions.

Compared to field investigation and experimentation, modeling can quantitatively estimate soil erosion more efficiently at large spatial and temporal scales (Ganasri and Ramesh 2016). This is especially true for highly heterogeneous environments such as karst areas, where it is expensive and unrealistic to monitor soil erosion under the wide range of environmental conditions. The universal soil loss equation (USLE) (Wischmeier and Smith 1978) or its revised form (RUSLE) (Renard et al. 1997) is a widely used empirical statistical model (Pope and Odhiambo 2014; Wu et al. 2016). The model is regularly used with geographic information systems (GIS) to predict and evaluate soil erosion at basin or larger scales, and it has been used in the karst geomorphology of both Cuba and China (Febles-Gonzalez et al. 2012; Xu et al. 2008). However, most applications in karst areas have neglected the blocking effect of miniature stone outcroppings at or near the surface. Firstly, due to the intercepting effect of exposed stones, the slope length factor, which accounts for soil erosion accumulation in RUSLE, is sensitive to the spatial resolution of the topographical data. More importantly, outcropping bedrocks and the thin soil layer usually result in soil erosion being lower in karst areas than in non-karst areas with similar latitudes (Feng et al. 2016). Therefore, the RUSLE model should be modified to suit karst areas by considering the relationship between soil erosion and bedrock bareness. For example, previous research revealed that simulation precision was related to the accumulated area threshold, and when this threshold (i.e., the grid cell size) was higher, the root mean square error was also higher (Feng et al. 2016). Thus, using high-resolution datasets could improve accuracy. In this study, high-resolution (9 m) digital elevation model (DEM) data were used.

The main objective of the present research was to modify the RUSLE model and identify the spatial gradient distribution and the dominant influencing factors of karst soil erosion. The specific aims of the study were (1) to provide more details of previous work about the RUSLE model and the problems in karst areas; (2) to modify the RUSLE model to suit karst areas; and (3) to discuss the spatial distribution of soil erosion and its dominant factors. It can be expected that the predicted large-scale soil erosion data and the dominant influencing factors determined in this study can provide a fundamental framework for amending erosion-related government policies.

Materials and methods

The study area was the Sancha River Basin (SRB), located between 104° 05' E–106° 06' E and 26° 02' N–27° 01' N (Fig. 1). It has an area of 4680 km² and is the source of the Wujiang River, which is the first branch of the Yangtze River. The karst peak-cluster depression is the most common geomorphology in the SRB. The area comprises of steep slopes, with 71% exceeding 5°, and elevation ranges from 939 to 2271 m. The steep terrain of the region, due to hydraulically eroded carbonate (i.e., dolomite and limestone), together with a subtropical monsoon climate, encourage the initiation of runoff and soil erosion. Total annual precipitation in 2015 ranged from 1044 to 1672 mm and was concentrated in May–October. Anthropogenic disturbances, such as overgrazing and deforestation, have caused increased vegetation changes and significantly

altered the vulnerable karst ecosystem, which has, in turn, aggravated regional poverty and formed a negative feedback loop between humans and the environment.

Dataset and methodology

Various datasets are needed for the RUSLE estimation. A DEM with a spatial resolution of 9 m was provided by Google Earth 6.0.3. The soil dataset (Fig. S1) with physical and chemical properties at a spatial resolution of 1 km was collected from the Harmonized World Database version 1.1 established by the Food and Agriculture Organization of the United Nations and the International Institute for Applied System Analysis. The data set was provided by Cold and Arid Regions Sciences Data Center at Lanzhou, China (<http://westdc.westgis.ac.cn>). Monthly precipitation observations

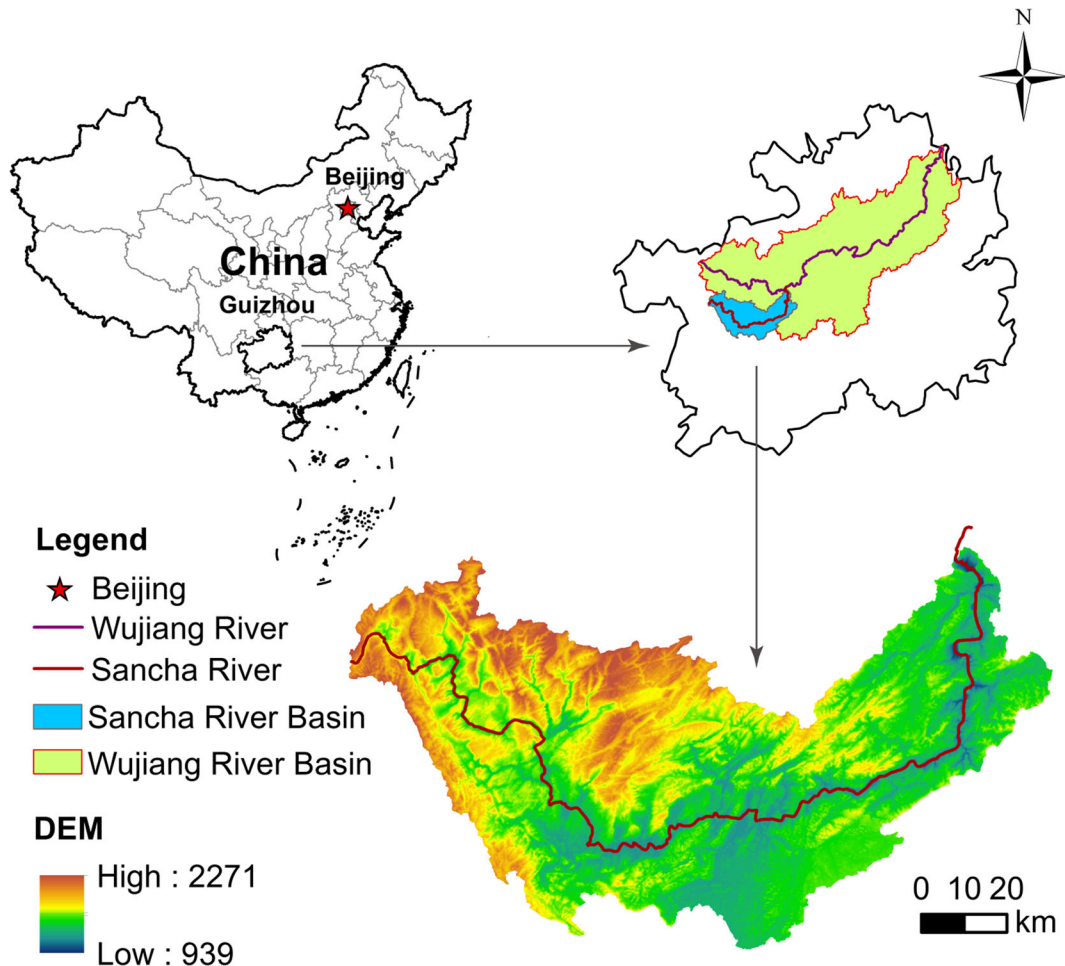


Fig. 1 The study area, the SRB, located in the Wujiang River Basin, Southwest China

during 2015 included data from 28 meteorological stations in the SRB and surrounding areas; these were obtained from the National Center of the China Meteorological Administration (CMA). A raster-gridded monthly precipitation dataset at 1 km resolution was obtained from the station observation data using ANUSPLIN software. This was developed using a “thin plate smoothing splines” algorithm, which interpolates climate variables as a function of latitude, longitude, and elevation (Mandal et al. 2016). The 2015 land use map, at a 30-m resolution, was interpreted from TM (thematic mapper) images by supervised classification methods with ENVI software based on field sampling points collected by GPS. The rocky desertification data were acquired from the State Forestry Administration (<http://www.forestry.gov.cn>).

Geomorphology and lithology data were downloaded from the Data Center for Resources and Environmental Sciences, Chinese Academy of Sciences (RESDC) (<http://www.resdc.cn>). The MODND1D normalized difference vegetation index with a spatial resolution of 500 m, acquired from the International Scientific & Technical Data Mirror Site, Computer Network Information Center, Chinese Academy of Sciences (<http://www.gscloud.cn>), was applied in this study to detect the influence of vegetation coverage on soil erosion.

The RUSLE model and its modification

The RUSLE model is an integrated reflection of natural and anthropogenic activities, including climate, soil characteristics, topographic factors, and man-made preventative actions. The model has been widely used to evaluate and estimate inter-rill and rill soil erosion (Renard et al. 1997). The mathematical equation is as follows:

$$A = R \times K \times LS \times C \times P \quad (1)$$

where A is the average annual soil loss due to water erosion ($t \text{ ha}^{-1} \text{ a}^{-1}$), R is the rainfall erosivity factor ($\text{MJ mm ha}^{-1} \text{ h}^{-1} \text{ a}^{-1}$), K is the erodibility factor ($\text{ha h MJ}^{-1} \text{ mm}^{-1} \text{ ha}^{-1}$), LS is the topographic factor, C is the cover and agricultural factor, and P is the conservation and supporting factor. LS , C , and P are dimensionless.

Due to the serious rocky desertification and shallow soils in karst areas, the RUSLE model usually

overestimates soil erosion rate and needs modification to improve the simulation accuracy. A previous study showed that soil erosion decreased with the increasing bedrock bareness (Wang et al. 2010a) because outcropping bedrocks can absorb rainwater, especially after long-term weathering (Xiong et al. 2012), and bedrocks have a resistance effect which reduces the surface runoff velocity (Kheir et al. 2008). Dai et al. (2017a), using artificial rainfall simulation, found that the correlation (R) between surface soil erosion and bedrock bareness rate was -0.076 ($P < 0.01$), which means that the relationship between surface soil erosion and bedrock bareness rate was significantly negative. The coefficient of determination (R^2) can measure how well soil erosion might be constructed from the bedrock bareness rate, and the multiplication of R^2 and the bedrock bareness rate can explain how much the bedrock bareness rate can contribute to soil erosion reduction. Thus, the multiplication of R^2 and the bedrock bareness rate was used to optimize the RUSLE model, by modifying Eq. (1) to Eq. (2).

$$\begin{aligned} A &= R \times K \times LS \times C \times P - (0.076^2 \times a) \times R \times K \times LS \times C \times P \\ &= (1 - 0.076^2 \times a) \times R \times K \times LS \times C \times P \end{aligned} \quad (2)$$

where a is the bedrock bareness rate in different degrees of rocky desertification, and the mean values were used to modify the RUSLE model (Table 1).

The R factor was influenced by the amount and intensity of rainfall, and was a function of rainfall characteristics. In China, the R factor was mostly simulated from monthly and annual precipitation data (Zha et al. 2015; Zeng et al. 2011). Wang and Jiao (1995) analyzed the distribution characteristics of the correlation coefficient between the R factor and rainfall parameters. They found that the rainfall quantity factor and the ratio of the sum of squares of monthly precipitation to annual precipitation had good correlations with the R factor in karst areas. Thus, the empirical equation for rainfall erosivity with monthly and annual precipitation, which was proposed by Wischmeier and Smith (1978), and revised by Arnoldus et al. (1980), was applied in this study. The method of the erosion-productivity impact calculator (EPIC) was used to calculate the K factor (Williams et al. 1989) with gridded soil property data, including sand (0.050–2.000 mm), silt particles (0.002–0.050 mm), clay (< 0.002 mm), and organic material content (%).

Table 1 Correctional coefficient for different degrees of rocky desertification (Li et al. 2006)

Rocky desertification	None	Potential	Light	Moderate	High	Severe
Bedrock bareness rate (%)	<20	20–30	31–50	51–70	71–90	>90
<i>a</i>	10	25	40	60	80	95

The *S* factor was computed based on McCool et al. (1987). The *L* factor calculation was based on the following expressions first proposed by McCool et al. (1989) and modified by Zhang et al. (2013a):

$$S = 10.8 \times \sin\theta + 0.03 \quad (\theta < 9\%, \lambda > 4.6m) \quad (3)$$

$$S = 16.8 \times \sin\theta - 0.50 \quad (\theta \geq 9\%, \lambda > 4.6m) \quad (4)$$

$$S = 3.0 \times (\sin\theta)^{0.8} + 0.56 \quad (\lambda < 4.6m) \quad (5)$$

$$L = \left(\frac{\lambda}{22.13}\right)^\alpha \quad (6)$$

$$\alpha = \left(\frac{\beta}{\beta + 1}\right) \quad (7)$$

$$\beta = \frac{\sin\theta}{3 \times (\sin\theta)^{0.8} + 0.56} \quad (8)$$

where θ is slope, λ is slope length, α is variable length-slope exponent, and β is a factor that varies with slope gradient.

The *C* and *P* factors showed strong spatial heterogeneity in different regions. Therefore, published values from karst areas were used for the calculations in the study area (Xu and Shao 2006; Feng et al. 2016; Xu et al. 2010; Zeng et al. 2017). The values of *C* and *P* factors are given in Table 2. The *C* value was originally acquired from field experiments, and it was the ratio of soil erosion with vegetation cover to soil erosion without vegetation cover (Cai et al. 2000).

Table 2 Values of *C* and *P* factors for different land use types

Land use types	Paddy land	Dry land	Forest land	Open forest	Shrub	Grassland	Water area	Construction land	Bare rock
<i>C</i>	0.1	0.22	0.006	0.01	0.01	0.04	0	0	0
<i>P</i>	0.15	0.4	1	1	1	1	0	0	1

The smaller the *C* value, the better the vegetation coverage conditions on the ground. *P* values were set to 0.15 and 0.4 for paddy land and dry land, respectively, and 1 for other land use types.

All the datasets were transformed to the projection of UTM/WGS84 and resampled at a spatial resolution of 30 m by the grid nesting method (Fig. S2).

Geographical detector method

The geographical detector method (Wang et al. 2010b) is a new statistical method, which can reveal the driving forces of an event by detecting spatially stratified heterogeneity. Four geographical detectors were developed based on spatial variation analysis of the geographical strata: factor detector, interaction detector, risk detector, and ecological detector. Factor detector and interaction detector were used in this study. The factor detector identified the power of influencing factors to determine soil erosion; it was measured by *q* value. The interaction detector indicated whether the influencing factors interacted or resulted in soil erosion independently. Multifactorial interaction between two factors can be explored by using the interaction detector module as follows: $q_{X1 \cap X2}$ means the *q* value of a new layer created by overlaying factor *X1* and *X2*. If $q_{X1 \cap X2} > q_{X1}$ or $q_{X1 \cap X2} > q_{X2}$, *X1* and *X2* enhance each other; if $q_{X1 \cap X2} > q_{X1} + q_{X2}$, they enhance each other nonlinearly; if $q_{X1 \cap X2} = q_{X1} + q_{X2}$, they are independent; if the $q_{X1 \cap X2} < q_{X1}$ or $q_{X1 \cap X2} < q_{X2}$, they weaken each other (more details about the geographical detector method can be found in Wang et al. 2010b).

Let Y be the variable of soil erosion, and X the layer of an influencing factor of soil erosion. The q value can be calculated with Eqs. (9) and (10). The geographical detector method deals with categorical independent variables, so X must be a categorical layer. The geomorphological type (Fig. S3a), lithology (Fig. S3b), and land use (Fig. S3c) were categorical variables; the other factors including elevation (Fig. 1), slope (Fig. S3d), rainfall (Fig. S3e), and vegetation coverage (Fig. S3f) were continuous raster, and the natural break method in ArcGis10.2 was used to put these data into nine discrete zones.

$$q = 1 - \frac{SSW}{SST} \quad (9)$$

$$SSW = \sum_{h=1}^L N_h \sigma_h^2 \quad SST = N \sigma^2 \quad (10)$$

where SSW means the sum of spatial variance of each zone, SST means global spatial variance of Y in the total area, L means the layer number of factor X , N_h and σ_h^2 represent the number of sample units and spatial variance of soil erosion in zone h , and N and σ^2 represent the number of global samples and variance, respectively.

Results and analysis

Model validation and soil erosion in SRB

The soil erosion rate in the SRB ranged from 0 to 167.60 t ha⁻¹a⁻¹ in 2015 (Fig. 2), with a mean value of 15.08 t ha⁻¹a⁻¹. These results were consistent with the values published by the water and soil conservation monitoring station in the Guizhou province, which reported that the average annual soil erosion in Guizhou was 13.61 t ha⁻¹a⁻¹. Other studies reported that soil erosion in a partially cultivated karst basin ranged from 14.4 to 28.7 t ha⁻¹a⁻¹ (Feng et al. 2016; Xu et al. 2008; Zeng et al. 2017). These results were all in agreement with the present study.

As displayed in Fig. 3, using the unmodified RUSLE model, with rocky desertification worsening, soil erosion showed an increasing trend. Soil erosion in moderate, high, and severe rocky desertification areas was 16.36, 20.10, and 16.76 t ha⁻¹a⁻¹ respectively. From moderate to high rocky desertification areas, soil erosion

increased by 22.8%, and from the moderate to severe rocky desertification areas, soil erosion increased by 2.3%. However, the soil was too shallow to induce enough erosion in the severe rocky desertification areas, and the simulation result was unreasonable. After modifying the RUSLE model, soil erosion increased by only 2.0% from moderate rocky desertification areas to high rocky desertification areas and decreased by 30.5% from moderate to severe rocky desertification areas. Besides, as the rocky desertification became worse, soil erosion displayed a decreasing trend in general, and the result was consistent with a recent study (Zeng et al. 2017).

Spatial gradient analysis of factors influencing soil erosion

Guizhou is a mountainous province with few plains, and the steep terrain has caused significant soil and water loss, even though there are numerous forests and other forms of vegetation cover. The land surface in the SRB is composed of five geomorphological types (Fig. S3a). Among these, the small relief mountains had the highest soil erosion rate (16.39 t ha⁻¹a⁻¹) (Fig. 4a), whereas the middle elevation plains had the lowest (9.47 t ha⁻¹a⁻¹), followed by the middle elevation terraces (9.63 t ha⁻¹a⁻¹). Soil erosion in the mountains was much higher than on the plains.

As observed in Fig. 4b, dolomite with clastic rocks was the lithology most vulnerable, with a soil erosion rate of up to 25.51 t ha⁻¹a⁻¹. By contrast, the interbedded limestone and dolomite and dolomite had the lowest risk of soil loss, with mean soil erosion of 11.56 and 13.96 t ha⁻¹a⁻¹, respectively. The average annual soil erosion of dolomite (13.69 t ha⁻¹a⁻¹) was lower than that of limestone (14.08 t ha⁻¹a⁻¹).

Figure 5a illustrates that soil erosion increased with altitude up to 1400–1600 m; when the elevation exceeded this level, soil erosion decreased. Figure 5b shows that soil erosion increased sharply with a greater slope gradient up to 25°, after which it increased at a much lower speed. Figure 5c shows that soil erosion increased sharply with increasing rainfall between 1200–1300 and 1300–1400 mm. When the annual rainfall was below 1100 mm, the soil erosion was at its lowest. However, once rainfall exceeded 1400 mm, soil erosion doubled.

A large part of the SRB was occupied by grassland and dry land (Fig. S3c). Dry land, with an average soil

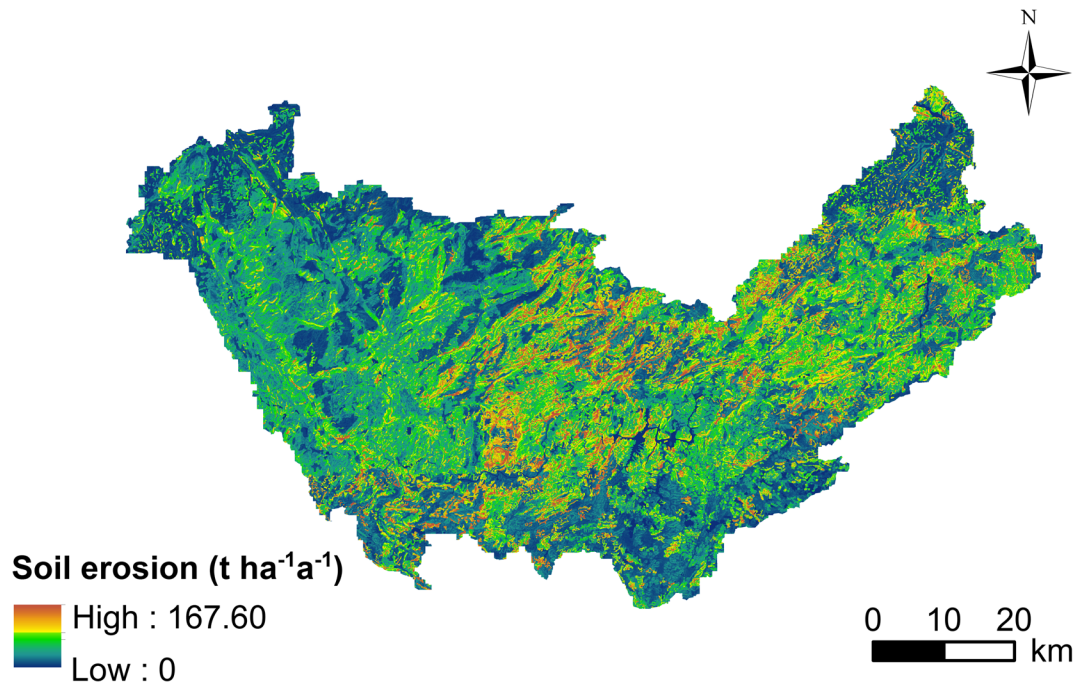


Fig. 2 Spatial pattern of soil erosion in the SRB in 2015

erosion rate of $30.54 \text{ t ha}^{-1} \text{ a}^{-1}$, was much more susceptible to soil erosion than other land use types (Fig. 6a). Areas of relatively flat land were so limited that dry lands were frequently cultivated on steep slopes to sustain the basic food requirements of the local population. These cultivated steep slopes were the main cause of significant soil loss. Soil erosion of the different land use types was ranked as follows: dry land > grassland > paddy land > open forest > shrub land > forest. Thus,

converting dry land and grasslands to forest, shrub, and open forest lands is a realistic and beneficial choice for soil conservation. As shown in Fig. 6b, with an increase in vegetation coverage, soil erosion increased until the vegetation coverage reached 0.5 to 0.6. The existence of a critical value is an essential feature in karst regions, distinguishing this landscape from other regions.

Multifactorial overlaying analysis between two influencing factors

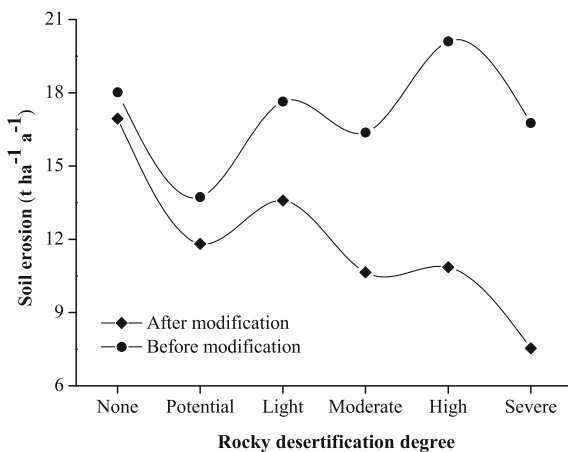
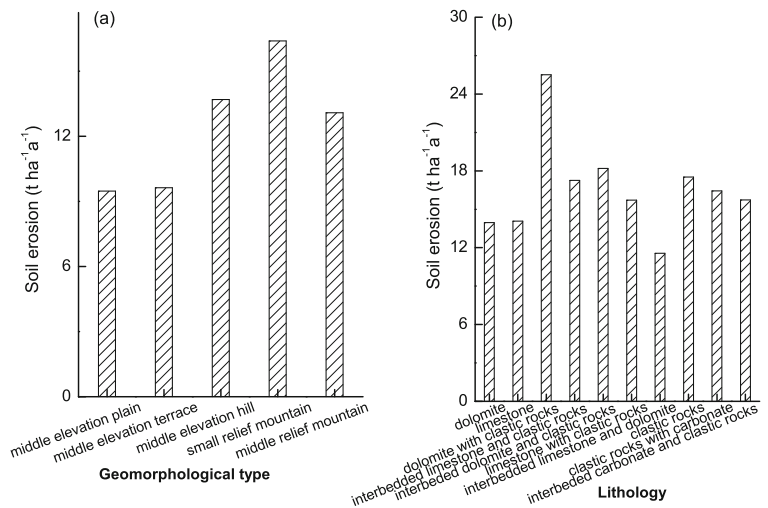


Fig. 3 Soil erosion under different degrees of rocky desertification in the SRB before and after model modification

As displayed in Fig. 7a, soil erosion differed for various land use types and slopes. For all land use types, soil erosion increased with increasing slope. Dry land was the most vulnerable to erosion, and with steeper slopes, soil erosion increased sharply for this land use type. Soil erosion was higher in dry land with slopes of between 10° and 15° than in paddy land, forest land, shrub land, open forest, construction land, or bare rock with slopes $> 35^\circ$. Figure 7b shows that soil erosion increased sharply with increasing slope when rainfall was higher than 1500 mm. When rainfall was below 1200 mm, soil erosion increased more slowly with increasing slope. When slope was lower than 20° , the differences between soil erosion under rainfall of 1100–1200 mm and 1200–1300 mm were not significant. However, with

Fig. 4 Average annual soil erosion ($\text{t ha}^{-1}\text{a}^{-1}$) in SRB (a) on different geomorphological types and SRB (b) on different lithology types in 2015



increasing slope, variation of soil erosion under different rainfall levels increased. In particular, a steep slope combined with higher rainfall aggravated soil erosion significantly.

Attribution analysis of soil erosion based on the geographical detector method

The geographical detector method was used to determine the dominant factors of soil erosion distribution. Although all of the factors discussed above were closely related to soil erosion, their contribution to the final result differed. The q values were ranked as follows: land use (0.51) > slope (0.10) > precipitation (0.06) > elevation (0.03) = lithology (0.03) > vegetation coverage (0.01) = geomorphology (0.01). Table 3 shows that all interactions between two influencing factors

enhanced each other, especially the combination of land use and slope, land use and rainfall, and slope and rainfall; the q values of these interactions were higher than the sum of the single factors, suggesting that their mutual enhancement was nonlinear. The interaction of land use and slope predominantly controlled soil erosion distribution, which can explain 68% of the soil erosion distribution in the SRB.

Discussion

Spatial heterogeneity of karst soil erosion

Due to the integrated influence of anthropogenic and natural factors, soil erosion showed a high spatial heterogeneity in the SRB. Soil erosion differed

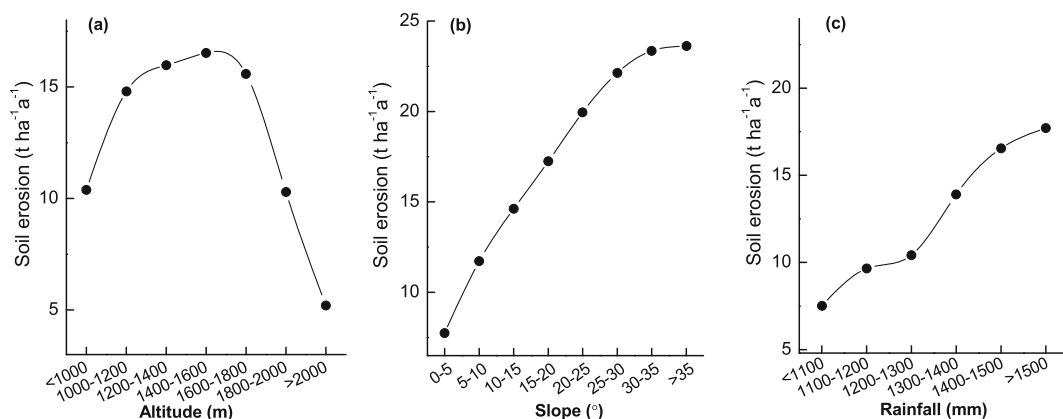
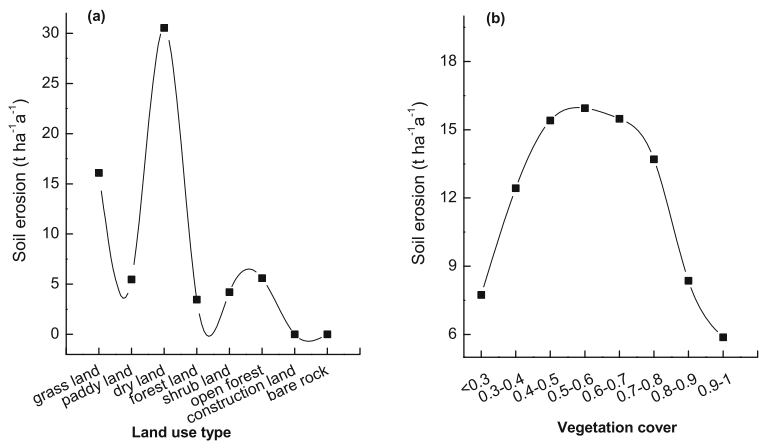


Fig. 5 Average annual soil erosion ($\text{t ha}^{-1}\text{a}^{-1}$) a at different elevations, b on different slopes, and c with different rainfall in the Sancha River Basin in 2015

Fig. 6 Average annual soil erosion ($t\ ha^{-1}\ a^{-1}$) for **a** different land use types and **b** different vegetation coverage in the SRB in 2015



considerably between different lithological types in this study, influenced by the composition of the surface evolving from the underlying stratigraphy (Zhang et al. 2013b), and soil non-erodibility also varied with different lithological types (Zhao et al. 2007). For example, soil erosion on limestone was higher than on dolomite because limestone is more easily eroded by water (Liu 2000). Moreover, geomorphology can affect the soil erosion rate indirectly by variation in the degree of land use (Zhao and Li 2016) and directly by the effect of topographical features, such as slope, slope length, and elevation (Kong et al. 2008). Soil erosion distribution in the SRB was consistent with slope distribution, and the most severe soil erosion occurred in areas where the gradient exceeded 25° , which may be linked to the vegetation pattern. The distribution characteristics of soil erosion on varied slopes differed from those of most non-karst regions. The grasses or shrubs were distributed on steep slopes covered by soil layers rather than over bare rocks, thus facilitating soil erosion under the combined effect of gravity and rainfall. Soil erosion

increased with increasing elevation, but when elevation exceeded 1400–1600 m, soil erosion decreased (Fig. 5a). As shown in Fig. S4, when elevation exceeded 1600 m, the area ratio of forest and shrub land, whose soil erosion was lower, increased sharply. At the same time, the area ratio of dry land, whose soil erosion was higher, decreased with elevation exceeding 1800 m, so soil erosion decreased when elevation exceeded 1600 m. Hence, in the areas at moderate elevation, anthropogenic activities had a significant impact on soil erosion, but in the areas at high elevation, human activities were restricted and soil erosion declined.

In addition, Wang et al. (2013) found that the relationship between vegetation coverage and soil erosion in karst regions differed from that of other regions. When the vegetation coverage was lower than a critical value, soil erosion increased with vegetation coverage, but once the coverage was above the critical value, soil erosion decreased with increased coverage. This critical threshold value in vegetation coverage was 0.5–0.6 in the Wujiang River Basin. In our study, similar results

Fig. 7 Soil erosion caused by the interactions of **a** land use and slopes, **b** rainfall and slopes in the SRB in 2015

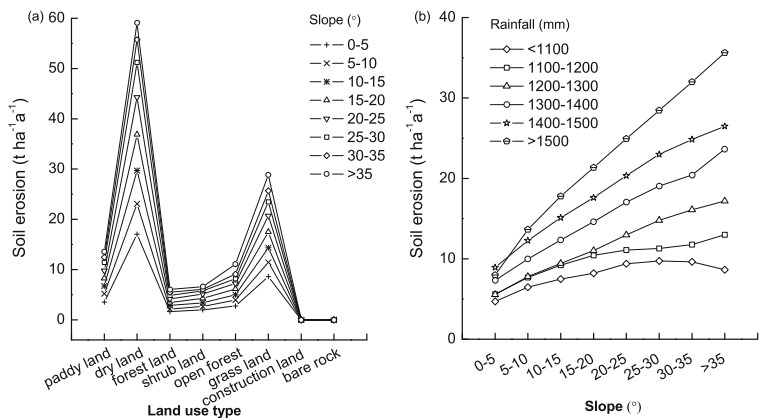


Table 3 The q values of factor interaction

	LU	Slope	Rainfall	VC	Elevation	Geomorphology	Lithology
LU	0.51						
Slope	0.68	0.10					
Rainfall	0.60	0.20	0.06				
VC	0.52	0.12	0.08	0.01			
Elevation	0.52	0.15	0.09	0.04	0.03		
Geomorphology	0.52	0.11	0.09	0.03	0.05	0.01	
Lithology	0.55	0.12	0.11	0.05	0.08	0.05	0.03

LU land use, VC vegetation coverage

were found. Vegetation coverage of 0.5–0.6 was the critical value in the SRB, which may be caused by the fact that water erosion is driven by either source-limited or transport-limited regimes (Kim et al. 2016). When the vegetation coverage was lower than 0.5–0.6, the occurrence and intensity of soil erosion showed source-limited characteristics, namely that the thin soil layer was the main limitation to soil erosion, and with the increase of vegetation coverage, the soil layer became thicker and soil erosion could therefore increase. However, when vegetation coverage exceeded 0.5–0.6, soil erosion exhibited transport-limited characteristics; with the vegetation coverage increasing, the canopy effectively intercepted rainfall and surface litter weakened the kinetic energy of raindrops, causing soil erosion to decline. As shown in Fig. S5, with the increasing vegetation coverage, the mean value of slope increased. When the vegetation coverage reached 0.5–0.6, the rate of slope increase was reduced, and with the increase in values of both slope and vegetation coverage, soil erosion decreased. This means that vegetation coverage played a more important role than slope in controlling soil erosion when vegetation coverage was higher than 0.5–0.6.

Interaction effects between impacting factors on soil erosion

Multifactorial interactions and their spatial patterns are key topics in geography. Previous research showed that land use, rainfall, and slope were the main single factors affecting soil erosion (Ganasri and Ramesh 2016; Peng and Wang 2012). This study showed that the interactions between land use and slope can explain 68% of the soil erosion distribution and thus predominantly

controlled it in the SRB. Soil erosion on the same slope with different land use types and on the same land use types with different slopes varied a lot, e.g., soil erosion in dry lands with slope of 0°–5° or in dry lands with slope of 15°–25°. In fact, karst areas mostly have dry lands in steeper zones (Peng and Wang 2012). For example, only 14.3% of the dry land was distributed in the areas with slopes of < 5° and approximately 33.4% of dry land occurred in the areas with slopes of > 15° in the SRB (Table 4). A steeper slope would significantly aggravate soil erosion in dry land areas, and in both dry and grass land areas, soil erosion increased more with increasing slope than in other land use types, especially where there were steep-slope tillage. It follows that the prohibition of steep-slope tillage is an important measure to reduce soil erosion. The combination of rainfall and slope significantly enhanced erosion. Once the rainfall increased from 1400–1500 to > 1500 mm, soil erosion increased sharply, especially in steeper areas. Consequently, to limit natural disasters, such as landslides and torrential floods, more attention should be given to steeper areas particularly during heavy rainfall events. It is therefore necessary to take extreme rainfall events into account by measuring their intensity and responding with timely and effective actions.

Uncertainty analysis and future perspective

In this study, we modified the RUSLE model to improve the accuracy by considering the influence of bedrock bareness on soil erosion, and using high-resolution (9 m) DEM data to improve the simulation precision of the LS factor. However, some limitations exist and need further study. First, the correlation coefficient of surface erosion and bedrock bareness was acquired from

Table 4 Area ratio of dry land in different slope gradients in 2015

Slope (°)	0–5	5–10	10–15	15–20	20–25	> 25
Area ratio (%)	14.3	26.6	25.7	16.5	9.3	7.6

artificial rainfall simulation tests, which was different to real conditions. Future studies should carry out field experiments to determine the exact relationship between soil erosion and bedrock bareness. Second, the equations used for the RUSLE factors affected on the results. For example, there are generally two kinds of methods to calculate the *C* factor. One method involves the *C* factor being calculated by NDVI data (Sun et al. 2014), in which case the accuracy may be affected by the spatial resolution, different geomorphological types, and the quality of satellite images. In karst areas especially, thick cloud will reduce the quality of satellite images, and the NDVI data can thus be inaccurate. Another is that the *C* factor could be given for different land use types; this method has been applied in most of the research in China karst areas (Xu et al. 2008; Feng et al. 2016). Due to that the *C* and *P* factors showed strong spatial heterogeneity in different regions, in this study, priority was given to the calculation of *C* and *P* factors in the karst areas (Xu and Shao 2006; Xu et al. 2010; Feng et al. 2016; Zeng et al. 2017). The *C* and *P* values were originally acquired based on the field experiment (Cai et al. 2000) and modified by Xu and Shao (2006) to suit karst areas. Although they can reflect the differences between different land use types and represent the degree of anthropogenic management, the spatial heterogeneity between different lithological and geomorphological types in karst areas was not considered enough. Thus, overall, the RUSLE parameters need refining in any future study.

Conclusion

Soil erosion showed high spatial heterogeneity in the karst region. The most severe soil erosion was concentrated at altitudes of 1200 to 1800 m, with dry and grass lands experiencing the higher rates. Middle elevation hills and dolomite with clastic rocks suffered from the most serious soil erosion. Rainfall provided the kinetic energy to cause soil erosion, so increased rainfall produced an increase in soil erosion. This study provided

further evidence that the relationship between vegetation coverage and soil erosion in karst landscapes hinges on a critical threshold. When the vegetation coverage exceeded 0.5 to 0.6, soil erosion decreased. According to the quantitative attribution analysis in the factor detector module, we concluded that soil erosion distribution was mostly controlled by anthropogenic activities, namely land use, followed by slope and rainfall.

Multifactorial interaction can enhance the impact of single factors on soil erosion. When dry and grass lands were combined with steep slopes, soil erosion increased dramatically. In addition, erosion increased sharply when high rainfall was combined with steep slopes. The dominant multifactorial interaction, based on the interaction detector module, was between land use and slope, which can explain 68% of soil erosion distribution. Our findings provide data that supports the return of farm lands to forests, especially on steep slopes where farmlands in the SRB are predominantly located. Additionally, more attention should be given to these steeper slope areas, in order to limit natural heavy rainfall events particularly during heavy rainfall events.

Funding information This research was financially supported by the National Basic Research Program of China (Grant No. 2015CB452702), the National Natural Science Foundation of China (Grant Nos. 41671098 and 41530749), and the “Strategic Priority Research Program” of the Chinese Academy of Sciences (Grant Nos. XDA20020202 and XDA19040304)

Publisher’s Note Springer Nature remains neutral with regard to jurisdictional claims in published maps and institutional affiliations.

References

Arnoldus, H. M. J., Boodt, M. D., & Gabriels, D. (1980). An approximation of the rainfall factor in the universal soil loss equation. In M. De Boodt & D. Gabriels (Eds.), *Assessment of erosion* (pp. 127–132). Chichester: Wiley.

Cai, C. F., Ding, S. W., Shi, Z. H., Huang, L., & Zhang, G. Y. (2000). Study of applying USLE and geographical information system IDRISI to predict soil erosion in small watershed. *Journal of Soil and Water Conservation*, 14(2), 19–24.

Chen, H. S., Yang, J., Fu, W., He, F., & Wang, K. L. (2012). Characteristics of slope runoff and sediment yield on karst hill-slope with different land-use types in northwest Guangxi. *Transactions of the Chinese Society of Agricultural Engineering*, 28(16), 121–126.

Dai, Q. H., Peng, X. D., Yang, Z., & Zhao, L. S. (2017a). Runoff and erosion processes on bare slopes in the karst rocky desertification area. *Catena*, 152, 218–226.

- Dai, Q. H., Peng, X. D., Zhao, L. S., Shao, H. B., & Yang, Z. (2017b). Effects of underground pore fissures on soil erosion and sediment yield on karst slopes. *Land Degradation & Development*, 28(7), 1922–1932. <https://doi.org/10.1002/ldr.2711>.
- Fang, G. L., Xiang, B., Zhao, W., Xie, Q., Diao, Z. Y., & Chi, W. F. (2015). Study on soil erosion in LaSa River basin based on GIS and RUSLE. *Journal of Soil and Water Conservation*, 29(3), 6–12.
- Febles-Gonzalez, J. M., Vega-Carreno, M. B., Tolon-Becerra, A., & Lastra-Bravo, X. (2012). Assessment of soil erosion in karst regions of Havana, Cuba. *Land Degradation & Development*, 23(5), 465–474. <https://doi.org/10.1002/ldr.1089>.
- Feng, T., Chen, H. S., Polyakov, V. O., Wang, K. L., Zhang, X. B., & Zhang, W. (2016). Soil erosion rates in two karst peak-cluster depression basins of northwest Guangxi, China: comparison of the RUSLE model with ¹³⁷Cs measurements. *Geomorphology*, 253, 217–224. <https://doi.org/10.1016/j.geomorph.2015.10.013>.
- Fu, B. J., Zhao, W. W., Chen, L. D., Zhang, Q. J., Lü, Y. H., Gulinck, H., et al. (2010). Assessment of soil erosion at large watershed scale using RUSLE and GIS: a case study in the Loess Plateau of China. *Land Degradation & Development*, 16(1), 73–85.
- Fu, B. J., Liu, Y., Lu, Y. H., He, C. S., Zeng, Y., & Wu, B. F. (2011). Assessing the soil erosion control service of ecosystems change in the Loess Plateau of China. *Ecological Complexity*, 8(4), 284–293. <https://doi.org/10.1016/j.ecocom.2011.07.003>.
- Fu, W., Huang, M. B., Gallichand, J., & Shao, M. G. (2012). Optimization of plant coverage in relation to water balance in the Loess Plateau of China. *Geoderma*, 173–174, 134–144. <https://doi.org/10.1016/j.geoderma.2011.12.016>.
- Ganasri, B. P., & Ramesh, H. (2016). Assessment of soil erosion by RUSLE model using remote sensing and GIS—a case study of Nethravathi Basin. *Geoscience Frontiers*, 7(6), 953–961. <https://doi.org/10.1016/j.gsf.2015.10.007>.
- Hu, Y. F., Tian, G. H., Mayer, A. L., & He, R. Z. (2015). Risk assessment of soil erosion by application of remote sensing and GIS in Yanshan Reservoir catchment, China. *Natural Hazards*, 79(1), 277–289. <https://doi.org/10.1007/s11069-015-1841-4>.
- Kheir, R. B., Abdallah, C., & Khawlie, A. (2008). Assessing soil erosion in Mediterranean karst landscapes of Lebanon using remote sensing and GIS. *Engineering Geology*, 99(3–4), 239–254. <https://doi.org/10.1016/j.enggeo.2007.11.012>.
- Kim, J., Ivanov, V. Y., & Fatichi, S. (2016). Environmental stochasticity controls soil erosion variability. *Scientific Reports*, 6. <https://doi.org/10.1038/srep22065>.
- Kong, Y. P., Zhang, K. L., & Cao, L. X. (2008). Appraise slope length factors in soil erosion study. *Research of Soil and Water Conservation*, 15(4), 43–47 52.
- Li, Y. B., Bai, X. Y., Zhou, G. F., LAN, A. J., Long, J., AN, Y. L., et al. (2006). The relationship of land use with karst rocky desertification in a typical karst area, China. *Acta Geographica Sinica*, 61(6), 624–632.
- Li, Y. B., Luo, G. J., Bai, X. Y., Wang, Y. Y., Wang, S. J., Xie, J., et al. (2014). The correlations among arable land, settlement and karst rocky desertification—cases study based on typical peak-cluster depression. *Acta Ecologica Sinica*, 34(9), 2195–2207.
- Liu, Z. H. (2000). Field experimental research on the corrosion kinetics of limestone and dolomite in allogenic water—case from Yaoshan Mt, Guilin. *Carsologica Sinica*, 19(1), 1–4.
- Long, T. W., Hunt, C. O., & Taylor, D. (2016). Radiocarbon anomalies suggest late onset of agricultural intensification in the catchment of the southern part of the Yangtze Delta, China. *Catena*, 147, 586–594. <https://doi.org/10.1016/j.catena.2016.08.017>.
- Mandal, S., Srivastav, R. K., & Simonovic, S. P. (2016). Use of beta regression for statistical downscaling of precipitation in the Campbell River basin, British Columbia, Canada. *Journal of Hydrology*, 538, 49–62. <https://doi.org/10.1016/j.jhydrol.2016.04.009>.
- Markose, V. J., & Jayappa, K. S. (2016). Soil loss estimation and prioritization of sub-watersheds of Kali River basin, Karnataka, India, using RUSLE and GIS. *Environmental Monitoring and Assessment*, 188(4). <https://doi.org/10.1007/s10661-016-5218-2>.
- McCool, D. K., Brown, L. C., Foster, G. R., Mutchler, C. K., & Meyer, L. D. (1987). Revised slope steepness factor for the universal soil loss equation. *Transactions of the Asae*, 30(5), 1387–1396.
- McCool, D. K., Foster, G. R., Mutchler, C. K., & Meyer, L. D. (1989). Revised slope length factor for the universal soil loss equation. *Transactions of the Asae*, 32(5), 1571–1576.
- Miller, J. D., Nyhan, J. W., & Yool, S. R. (2003). Modeling potential erosion due to the Cerro Grande Fire with a GIS-based implementation of the revised universal soil loss equation. *International Journal of Wildland Fire*, 12(1), 85–100. <https://doi.org/10.1071/wf02017>.
- Parise, M., De Waele, J., & Gutierrez, F. (2008). Current perspectives on the environmental impacts and hazards in karst. *Environmental Geology*, 58(2), 235–237. <https://doi.org/10.1007/s00254-008-1608-2>.
- Peng, T., & Wang, S. J. (2012). Effects of land use, land cover and rainfall regimes on the surface runoff and soil loss on karst slopes in southwest China. *Catena*, 90(1), 53–62.
- Pope, I. C., & Odhiambo, B. K. (2014). Soil erosion and sediment fluxes analysis: a watershed study of the Ni Reservoir, Spotsylvania County, VA, USA. *Environmental Monitoring and Assessment*, 186(3), 1719–1733. <https://doi.org/10.1007/s10661-013-3488-5>.
- Renard, K. G., Foster, G. R., Weesies, G. A., McCool, D. K., & Yoder, D. C. (1997). *Predicting soil erosion by water: a guide to conservation planning with the revised universal soil loss equation (RUSLE) (agriculture handbook)*. Washington, DC: USDA.
- Sun, W. Y., Shao, Q. Q., Liu, J. Y., & Zhai, J. (2014). Assessing the effects of land use and topography on soil erosion on the Loess Plateau in China. *Catena*, 121, 151–163.
- Wang, W. Z., & Jiao, J. Y. (1995). Study on rainfall erosivity in China (I). *Journal of Soil and Water Conservation*, 9(4), 5–18.
- Wang, J., Cai, X. F., Lei, L., & Zhang, H. (2010a). Laboratory simulation on soil erosion under different bedrock outcrop rate in southwest karst area, China. *Carsologica Sinica*, 29(1), 1–5.
- Wang, J. F., Li, X. H., Christakos, G., Liao, Y. L., Zhang, T., Gu, X., & Zheng, X. Y. (2010b). Geographical detectors-based

- health risk assessment and its application in the neural tube defects study of the Heshun region, China. *International Journal of Geographical Information Science*, 24(1), 107–127. <https://doi.org/10.1080/13658810802443457>.
- Wang, Y., Cai, Y. L., & Pan, M. (2013). Analysis on the relationship between soil erosion and land use in Wujiang River basin in Guizhou Province. *Research of Soil and Water Conservation*, 20(3), 11–18.
- Wang, W. J., Deng, R. X., & Zhang, S. W. (2014). Preliminary research on risk evaluation of gully erosion in typical black soil area of Northeast China. *Journal of Natural Resources*, 29(12), 2058–2067.
- Wang, Y., Zhang, J. H., Zhang, Z. H., & Jia, L. Z. (2016). Impact of tillage erosion on water erosion in a hilly landscape. *Sci Total Environ*, 551–552, 522–532. <https://doi.org/10.1016/j.scitotenv.2016.02.045>.
- Williams, J. R., Jones, C. A., Kiniry, J. R., & Spanel, D. A. (1989). The EPIC crop growth-model. *Transactions of the Asae*, 32(2), 497–511.
- Wischmeier, W., & Smith, D. (1978). *Predicting rainfall erosion losses: a guide to conservation planning (agriculture handbook)*. Washington, DC: USDA.
- Wu, L., Liu, X., & Ma, X. Y. (2016). Spatiotemporal distribution of rainfall erosivity in the Yanhe River watershed of hilly and gully region, Chinese Loess Plateau. *Environmental Earth Sciences*, 75(4). <https://doi.org/10.1007/s12665-015-5136-6>.
- Xiong, K. N., Li, J., & Long, M. Z. (2012). Features of soil and water loss and key issues in demonstration areas for combating karst rocky desertification. *Acta Geographica Sinica*, 67(7), 878–888.
- Xu, Y. Q., & Shao, X. M. (2006). Estimation of soil erosion supported by GIS and RUSLE: a case study of Maotiaohe Watershed, Guizhou Province. *Journal of Beijing Forestry University*, 28(4), 67–71.
- Xu, Y. Q., Shao, X. M., Kong, X. B., Peng, J., & Cai, Y. L. (2008). Adapting the RUSLE and GIS to model soil erosion risk in a mountains karst watershed, Guizhou Province, China. *Environmental Monitoring and Assessment*, 141(1–3), 275–286. <https://doi.org/10.1007/s10661-007-9894-9>.
- Xu, Y. Q., Huang, J., Feng, Y., & Zhou, D. (2010). Soil erosion economic loss under different land use structures: a case study of Maotiao River Watershed, Guizhou Province. *Progress in Geography*, 29(11), 1451–1456.
- Xu, Q. Y., Huang, M., Liu, H. S., & Yan, H. M. (2011). Integrated assessment of eco-environmental vulnerability in Pearl River Delta based on RS and GIS. *The Journal of Applied Ecology*, 22(11), 2987–2995.
- Yu, H. Q., Li, Y., Zhou, N., Chappell, A., Li, X. Y., & Poesen, J. (2016). Soil nutrient loss due to tuber crop harvesting and its environmental impact in the North China Plain. *Journal of Integrative Agriculture*, 15(7), 1612–1624. [https://doi.org/10.1016/s2095-3119\(15\)61268-0](https://doi.org/10.1016/s2095-3119(15)61268-0).
- Zeng, L. Y., Wang, M. H., & Li, C. M. (2011). Study on soil erosion and its spatio-temporal change at Hongfeng Lake watershed based on RUSLE model. *Hydrogeology & Engineering Geology*, 32(2), 113–118.
- Zeng, C., Wang, S. J., Bai, X. Y., Li, Y. B., Tian, Y. C., Li, Y., et al. (2017). Soil erosion evolution and spatial correlation analysis in a typical karst geomorphology using RUSLE with GIS. *Solid Earth*, 8(4), 1–26.
- Zha, L. S., Deng, G. H., & Gu, J. C. (2015). Dynamic changes of soil erosion in the Chaohu Watershed from 1992 to 2013. *Acta Geographica Sinica*, 70(11), 1708–1719.
- Zhang, H. M., Yang, Q. K., Li, R., Liu, Q. R., Moore, D., He, P., et al. (2013a). Extension of a GIS procedure for calculating the RUSLE equation LS factor. *Computers & Geosciences*, 52, 177–188. <https://doi.org/10.1016/j.cageo.2012.09.027>.
- Zhang, X. B., Wang, S. J., Bai, X. Y., Chen, W. Y., & Zhang, S. Y. (2013b). Relationships between the spatial distribution of karst land desertification and geomorphology, lithology, precipitation, and population density in Guizhou Province. *Earth and Environment*, 41(1), 1–6.
- Zhao, Y., & Li, X. (2016). Spatial correlation between type of mountain area and land use degree in Guizhou Province, China. *Sustainability*, 8(9). <https://doi.org/10.3390/su8090849>.
- Zhao, Y. Y., Zhou, Y. C., & Duan, X. (2007). Anti-erodibility and anti-scourability of different lithological soils in karst area of Central Guizhou Province. *Journal of Anhui Agricultural Sciences*, 35(29), 9311–9313 9317.